Research Article | Vol. 26, No. 20 | 1 Oct 2018 | OPTICS EXPRESS 25645
Optics EXPRESS

High signal-to-noise ratio ultra-compact lab-on-a-chip microflow cytometer enabled by silicon optical antennas

SERGIO LECHAGO,* CARLOS GARCÍA-MECA, NURIA SÁNCHEZ-LOSILLA, AMADEU GRIOL, AND JAVIER MARTÍ

Nanophotonics Technology Center, Universitat Politècnica de València, 46022 Valencia, Spain
**serlecbu@ntc.upv.es*

Abstract: We experimentally demonstrate an all-silicon nanoantenna-based micro-optofluidic cytometer showing a combination of high signal-to-noise ratio (SNR) > 14 dB and ultra-compact size. Thanks to the ultra-high directivity of the antennas (>150), which enables a state-of-the-art sub-micron resolution, we are able to avoid the use of the bulky devices typically employed to collimate light on chip (such as lenses or fibers). The nm-scale antenna cross section allows a dramatic reduction of the optical system footprint, from the mm-scale of previous approaches to a few μm^2, yielding a notable reduction in the fabrication costs. This scheme paves the way to ultra-compact lab-on-a-chip devices that may enable new applications with potential impact on all branches of biological and health science.

OCIS codes: (130.0130) Integrated optics; (280.1415) Biological sensing and sensors; (350.4238) Nanophotonics and photonic crystals.

References and links

1. B. Redding, S. F. Liew, R. Sarma, and H. Cao, "Compact spectrometer based on a disordered photonic chip," Nat. Photonics **7**(8), 746–751 (2013).
2. M. Malinauskas, A. Žukauskas, S. Hasegawa, Y. Hayasaki, V. Mizeikis, R. Buividas, and S. Juodkazis, "Ultrafast laser processing of material: from science to industry," Light Sci. Appl. **5**(8), e16133 (2016).
3. X. Fan and I. M. White, "Optofluidic microsystems for chemical and biological analysis," Nat. Photonics **5**(10), 591–597 (2011).
4. N. I. Zheludev and Y. S. Kivshar, "From metamaterials to metadevices," Nat. Mater. **11**(11), 917–924 (2012).
5. Y. S. Zhang, B. R. Watts, T. Y. Guo, Z. Y. Zhang, C. Q. Xu, and Q. Fang, "Optofluidic device based microflow cytometers for particle/cell detection: a review," Micromachines (Basel) **7**(4), 70 (2016).
6. X. Chen, C. Li, and H. K. Tsang, "Device engineering for silicon photonics," NPG Asia Mater. **3**(1), 34–40 (2011).
7. G. Luka, A. Ahmadi, H. Najjaran, E. Alocilja, M. DeRosa, K. Wolthers, A. Malki, H. Aziz, A. Althani, and M. Hoorfar, "Microfluidics Integrated Biosensors: A Leading Technology towards Lab-on-a-Chip and Sensing Applications," Sensors (Basel) **15**(12), 30011–30031 (2015).
8. M. Padgett and R. Bowman, "Tweezers with a twist," Nat. Photonics **5**(6), 343–348 (2011).
9. Y. Shiau, "Dielectric Rod Antennas for Millimeter-Wave Integrated Circuits," IEEE Trans. Microw. Theory Tech. **24**(11), 869–872 (1976).
10. H. Zhou, Z. Li, L. Shang, A. Mickelson, and D. S. Filipovic, "On-Chip Wireless Optical Broadcast Interconnection Network," J. Lightwave Technol. **28**(24), 3569–3577 (2010).
11. M. L. Brongersma, "Plasmonics: Engineering optical antennas," Nat. Photonics **2**(5), 270–272 (2008).
12. A. Alù and N. Engheta, "Wireless at the Nanoscale: Optical Interconnects using Matched Nanoantennas," Phys. Rev. Lett. **104**(21), 213902 (2010).
13. L. Novotny and N. van Hulst, "Antennas for light," Nat. Photonics **5**(2), 83–90 (2011).
14. V. Giannini, A. I. Fernández-Domínguez, S. C. Heck, and S. A. Maier, "Plasmonic Nanoantennas: Fundamentals and Their Use in Controlling the Radiative Properties of Nanoemitters," Chem. Rev. **111**(6), 3888–3912 (2011).
15. J. Sun, E. Timurdogan, A. Yaacobi, E. S. Hosseini, and M. R. Watts, "Large-scale nanophotonic phased array," Nature **493**(7431), 195–199 (2013).
16. K. Van Acoleyen, H. Rogier, and R. Baets, "Two-dimensional optical phased array antenna on silicon-on-insulator," Opt. Express **18**(13), 13655–13660 (2010).
17. C. García-Meca, S. Lechago, A. Brimont, A. Griol, S. Mas, L. Sánchez, L. Bellieres, N. S. Losilla, and J. Martí, "On-chip wireless silicon photonics: from reconfigurable interconnects to lab-on-chip devices," Light Sci. Appl. **6**(9), e17053 (2017).
18. J. P. Robinson and M. Roederer, "Flow cytometry strikes gold," Science **350**(6262), 739–740 (2015).

#330169 https://doi.org/10.1364/OE.26.025645
Journal © 2018 Received 24 Apr 2018; revised 1 Jun 2018; accepted 2 Jun 2018; published 18 Sep 2018

Optics EXPRESS

19. X. Mao, A. A. Nawaz, S. C. Lin, M. I. Lapsley, Y. Zhao, J. P. McCoy, W. S. El-Deiry, and T. J. Huang, "An integrated, multiparametric flow cytometry chip using "microfluidic drifting" based three-dimensional hydrodynamic focusing," Biomicrofluidics **6**(2), 24113 (2012).
20. N. T. Huang, H. L. Zhang, M. T. Chung, J. H. Seo, and K. Kurabayashi, "Recent advancements in optofluidics-based single-cell analysis: optical on-chip cellular manipulation, treatment, and property detection," Lab Chip **14**(7), 1230–1245 (2014).
21. D. Psaltis, S. R. Quake, and C. Yang, "Developing optofluidic technology through the fusion of microfluidics and optics," Nature **442**(7101), 381–386 (2006).
22. K. C. Cheung, M. Di Berardino, G. Schade-Kampmann, M. Hebeisen, A. Pierzchalski, J. Bocsi, A. Mittag, and A. Tárnok, "Microfluidic Impedance-Based Flow Cytometry," Cytometry A **77**(7), 648–666 (2010).
23. K. Cheung, S. Gawad, and P. Renaud, "Impedance Spectroscopy Flow Cytometry: On-Chip Label-Free Cell Differentiation," Cytometry A **65**(2), 124–132 (2005).
24. X. Xie, Z. Cheng, Y. Xu, R. Liu, Q. Li, and J. Cheng, "A sheath-less electric impedance micro-flow cytometry device for rapid label-free cell classification and viability testing," Anal. Methods **9**(7), 1201–1212 (2017).
25. T. Blasi, H. Hennig, H. D. Summers, F. J. Theis, J. Cerveira, J. O. Patterson, D. Davies, A. Filby, A. E. Carpenter, and P. Rees, "Label-free cell cycle analysis for high-throughput imaging flow cytometry," Nat. Commun. **7**, 10256 (2016).
26. P. Van Zant, *Microchip Fabrication: A Practical Guide to Semiconductor Processing* (McGraw Hill Education, 2014).
27. R. Voelkel, "Wafer-scale micro-optics fabrication," Adv. Opt. Technol. **1**(3), 135–150 (2012).
28. R. Soref, "The Past, Present, and Future of Silicon Photonics," IEEE J. Quantum Electron. **12**(6), 1678–1687 (2006).
29. O. Kononchuk and B. Y. Nguyen, *Silicon-on-insulator (SOI) technology: Manufacture and applications* (Elsevier, 2014).
30. R. Baets, P. Dumon, W. Bogaerts, G. Roelkens, D. Taillaert, B. Luyssaert, G. Priem, G. Morthier, P. Bienstman, and D. Van Thourhout, "Silicon-on-insulator based nano-photonics: Why, How, What for?" in *2nd IEEE International Conference Group IV Photonics* (IEEE, 2005), pp. 168–170.
31. M. Frankowski, J. Theisen, A. Kummrow, P. Simon, H. Ragusch, N. Bock, M. Schmidt, and J. Neukammer, "Microflow Cytometers with Integrated Hydrodynamic Focusing," Sensors (Basel) **13**(4), 4674–4693 (2013).
32. D. Barat, D. Spencer, G. Benazzi, M. C. Mowlem, and H. Morgan, "Simultaneous high speed optical and impedance analysis of single particles with a microfluidic cytometer," Lab Chip **12**(1), 118–126 (2012).
33. G. Testa, G. Persichetti, and R. Bernini, "Micro flow cytometer with self-aligned 3D hydrodynamic focusing," Biomed. Opt. Express **6**(1), 54–62 (2014).
34. S. Etcheverry, A. Faridi, H. Ramachandraiah, T. Kumar, W. Margulis, F. Laurell, and A. Russom, "High performance micro-flow cytometer based on optical fibres," Sci. Rep. **7**(1), 5628 (2017).
35. C. A. Balanis, *Antenna Theory: Analysis and Design* (Wiley, 1982).
36. T. Kosako, Y. Kadoya, and H. F. Hofmann, "Directional control of light by a nano-optical Yagi-Uda antenna," Nat. Photonics **4**(5), 312–315 (2010).
37. K. T. Kotz, A. C. Petrofsky, R. Haghgooie, R. Granier, M. Toner, and R. G. Tompkins, "Inertial focusing cytometer with integrated optics for particle characterization," Technology (Singap World Sci) **1**(1), 27–36 (2013).
38. D. Taillaert, F. Van Laere, M. Ayre, W. Bogaerts, D. Van Thourhout, P. Bientsman, and R. Baets, "Grating Couplers for Coupling between Optical Fibers and Nanophotonic Waveguides," Jpn. J. Appl. Phys. **45**(8A), 6071–6077 (2006).
39. M. C. Potcoava, G. L. Futia, J. Aughenbaugh, I. R. Schlaepfer, and E. A. Gibson, "Raman and coherent anti-Stokes Raman scattering microscopy studies of changes in lipid content and composition in hormone-treated breast and prostate cancer cells," J. Biomed. Opt. **19**(11), 111605 (2014).
40. M. C. Traub, W. Longsine, and V. N. Truskett, "Advances in Nanoimprint Lithography," Annu. Rev. Chem. Biomol. Eng. **7**(1), 583–604 (2016).
41. B. B. Xu, Y. L. Zhang, H. Xia, W. F. Dong, H. Ding, and H. B. Sun, "Fabrication and multifunction integration of microfluidic chips by femtosecond laser direct writing," Lab Chip **13**(9), 1677–1690 (2013).
42. R. M. Zucker, J. N. R. Ortenzio, and W. K. Boyes, "Characterization, Detection, and counting of Metal Nanoparticles Using Flow Cytometry," Cytometry A **89**(2), 169–183 (2016).
43. B. Kowalczyk, I. Lagzi, and B. A. Grzybowski, "Nanoseparation: Strategies for size and/or shape-selective purification of nanoparticles," Curr. Opin. Colloid Interface Sci. **16**(2), 135–148 (2011).

1. Introduction

The relentless progress of photonic integrated technology has enabled a vast catalogue of new applications able to bring solutions not only in the traditional fields of communications or computing, but also in other areas such as spectroscopy [1], beam shaping and advanced material processing [2], or biomedicine [3]. Along this line, we have witnessed how this technology has sparked the development of metadevices [4] and point-of-care (POC) lab-on-a-chip sensors [5], amongst many others. Traditionally, photonic circuits are built upon

Optics EXPRESS

waveguide-based layout implementations, an acceptable feature for many systems [6], but that in turn provide harsh design rules and usually lead to complex and non-compact device footprints. Additionally, the inherent confined nature of the electromagnetic fields travelling within or over photonic wires limits their ability to interact with the surrounding medium at far-field distances. This stringent characteristic prevents their use in several kinds of biosensors and devices [7], as well as in other applications as, for instance, those related to dynamic microparticle control [8].

The possibility of using wireless devices on a chip has been proposed as an alternative to the typically widespread waveguide-based schemes [9–17]. These new wireless systems usually rely on the use of optical nanoantennas, which are able to radiate within a chip, aping the behavior of radiofrequency or microwave antennas. Most of the wireless implementations found in the literature are based on the use of plasmonic nanoantennas [11–14], a suitable solution to concentrate optical energy in the visible or near-infrared spectrum. Moreover, these devices would potentially enable a bridge to quantum systems or single-photon sources [13], showing a better efficiency than plasmonic nanowires. However, these wireless devices still display strong absorption losses and a poor radiation performance in high frequency bands. Other approaches employ dielectric antennas in grating coupler [15, 16] configurations, only suitable for off-chip interconnects.

Very recently, a new kind of on-chip photonic silicon antenna with a tremendously improved radiation performance was proposed, showing directivities higher than 150 (linear units) and total efficiencies close to 90% [17]. Moreover, these dielectric antennas provide low losses and a wide working bandwidth at the telecom wavelengths, while the use of silicon as the constituent material assures their compatibility with the complementary metal-oxide-semiconductor (CMOS) technology. These devices have experimentally proved their suitability as the main building block in several experimental applications ranging from dynamically-reconfigurable wireless pathways to lab-on-a-chip flow cytometers, the object of the present study. Flow cytometry allows the rapid and simultaneous analysis of multiple parameters of live cells in a heterogeneous mix as they flow in a stream through optical or electric signals. This technique has become an essential tool in cell sorting and analysis, with a paramount importance in the treatment of diseases such as AIDS or cancer [18]. However, traditional flow cytometers are expensive (with a price that can be of the order of 100.000 US$ for a single unit [19]) and require the presence of specialized staff in their use, implying additional indirect costs. Moreover, traditional flow cytometers demand large amounts of expensive reagents, with complicated processing steps, feature that also entails high maintenance costs [5]. Lab-on-a-chip technology is a promising alternative for reducing the cost of biomedical equipment while presenting, at the same time, additional advantages such as yielding more compact implementations [20, 21]. As a consequence, there has been an intense research activity to achieve integrated lab-on-a-chip cytometers that use microfluidic technology (microflow cytometers) during the last 15 years [5, 20].

Flow and microflow cytometry usually relies on the use of optical- or impedance-based technology [5, 22]. While both schemes offer valuable and complementary information [22], impedance-based systems present some disadvantages as compared to optical ones. For instance, an impedance-based multiparametric analysis can only be performed by using alternating electric current signals with different frequencies, which requires the presence of external function generators and amplifiers [23]. In contrast, this can be achieved with optical cytometers just by scanning different angles at a single frequency. Moreover, the use of electric currents entails the possibility of damaging the analyte [24]. Additionally, impedance microflow cytometers require the integration of electrodes into the microfluidic channel, which increases the cost and complexity of the device as compared to optical approaches [20]. Furthermore, the metals commonly used to fabricate the electrodes, such as platinum [23] are not CMOS compatible. Most of the current approaches to on-chip microflow cytometry are based on optofluidic devices [5], which synergistically combine integrated

Optics EXPRESS

photonics with microfluidics in a single chip (termed optofluidic chip) to count, sort or analyze flows of live cells. Within the optical approach, fluorescence and scattering cytometry have been extensively discussed in the literature [5]. Fluorescence-based flow cytometry has proved to be a reliable technique to identify and classify biotargets. However, current trends in microflow cytometry are leading to label-free systems [25], as they avoid the cost, time, and required training associated with the labelling process, as well as the use of fluorescent biomarkers that could potentially damage the analyte. To a large extent, research efforts along this line have addressed the miniaturization and the improvement of the integration level of the optical and fluidic subsystems, in order to reduce the cost and enhance portability.

Regarding the optical subsystem, on which we focus in this paper, state-of-the-art on-chip optofluidic microcytometers rely on the use of fibers or microlenses to illuminate the sample and collect the scattered light [5], as this avoids the use of expensive external optical elements and facilitates the alignment of the different system components, as well as the sought size reduction, all of which contribute to minimize costs. Despite the fact that fiber-based devices suppose a notable advance in portability and cost reduction with respect to standard cytometers, the use of fibers requires complex fabrication and packaging steps that hamper the automation of the fabrication process, limiting the cost reduction. Moreover, optical fibers are a source of potential losses and failure at discrete component interfaces. The key to achieve a drastic cost reduction would be to develop devices that can be completely fabricated using standard wafer-scale manufacturing approaches, such as the CMOS technology employed for the production of integrated circuits, which relies on planar processes that allow the automatic fabrication of many devices in parallel [26]. Microlens-based optical subsystems are compatible with this approach, representing a lower cost option than fiber-based cytometers [27].

Furthermore, in wafer-scale manufacturing, a reduction of the size of the chip directly decreases its fabrication cost (as well as indirectly, since the tolerance to fabrication defects increases) [26]. In this sense, the solution proposed in [17] is based on integrated silicon nanoantennas with a footprint as small as 0.64×14 μm^2, representing, to our knowledge, the most compact optical subsystem for a microflow cytometer to date, with a notable size reduction (up to four orders of magnitude) with respect to previous approaches [5]. This feature, together with the fact that the proposed structures can be fabricated using standard CMOS-compatible silicon-on-insulator (SOI) technology [28, 29] (the best planar fabrication technology for optical chips in many aspects [30]), shows the low-cost nature of this approach. Achieving this level of miniaturization is also important to improve portability, as well as to increase the number of parallel analyses that can be performed within the same chip, and enables a fine angular field sampling. Moreover, the ultra-directive nature of these structures renders a state-of-the-art particle resolution, exemplified by the experimental characterization and classification of polystyrene microspheres with a diameter as small as 1 μm. Obviously, employing fully integrated antennas inherently avoids the use of fibers and external bulky optical elements usually employed to focus light on chip [31–34]. As a consequence, these silicon nanoantennas emerge as an interesting alternative that may supersede microlenses and optical fibers for the realization of low-cost lab-on-a-chip microflow cytometers. Here, taking this previous work a step further, we design and experimentally demonstrate an on-chip microfluidic nanoantenna-based microflow cytometer with a significantly improved SNR (a fundamental parameter that establishes the ability of the device to resolve targets from the noise level), outperforming most previous integrated microflow cytometers [5]. To this end, we looked for the reception antenna angle that maximizes the SNR, finding a good agreement between simulations and experiments. The employed configuration constitutes a much more compact version than previous designs [5, 31–34] and competes with the best state-of-the- art SNR shown so far with a label-free detection scheme. Additionally, this implementation provides a very low coefficient of

Optics EXPRESS

variation (CV) for specific angular directions. All designs and experiments correspond to a wavelength λ = 1550 nm.

2. Theoretical results and discussion

We start by reviewing the working principle of the employed all-silicon nanoantennas, upon which the optical subsystem of the device is built. In particular, we used the antennas proposed [17], which are based on open-ended strip waveguides. The directivity of these structures was modelled via Huygens' principle, following the method typically used in classic microwave and radiofrequency theory [35]. This approach directly links the nanowire radiation pattern with the Fourier transform of its mode transverse electric and magnetic fields. A straightforward implication is that less confined modes lead to higher directivities, since the angular extension of the radiation vectors decreases as the spatial extension of the mode increases [17]. It was proved that by varying the transverse dimension of these strip wires, the mode confinement can be tuned, thus providing an easy way of tailoring the final directivity of the waveguide-based antenna. In the final configuration of the microflow cytometer we use an antenna consisting of a transition from a standard 450-nm-width 220-nm-height strip silicon wire to a 150-nm-width silicon tip through an inverted taper, which already achieves a directivity as high as 54 (linear units), see Fig. 1(a). Several additional elements (the so-called directors) were placed in front of the antenna to further improve its directivity [17, 36]. Figure 1(a) shows the impact of the number of directors on the antenna directivity. The final configuration is an inverted taper nanoantenna with two directors, see Fig. 1(b), yielding a directivity of 114, enough to fulfil the requirements of our upcoming experiments.

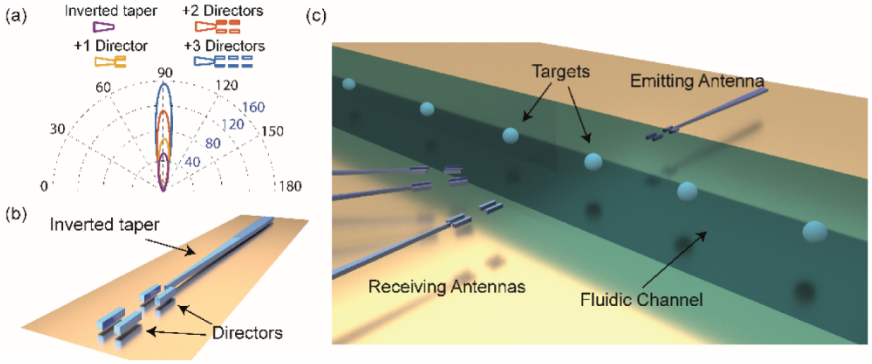

Fig. 1. (a) Polar directivity diagram of the designed antennas as a function of the number of directors. Blue numbers represent the directivity value while black numbers account for the angular directions. (b) Artwork displaying the final antenna configuration used for the experimental microflow cytometer, made up of a silicon inverted taper nanoantenna and two directors. A 2-μm thick layer of SiO_2 covered the antennas in the experiments. (c) Scheme of the proposed microflow cytometer based on the use of the designed silicon antennas. The targets flow within the microchannel and the characteristic scattered pulse is retrieved at the receiving set of antennas.

As mentioned before, the ultra-high directive nature of this structure, able to radiate most of the power in a small range of angular directions, avoids the need for bulky devices, such as lenses or multimode interference devices, to produce the needle-like beams required in high-resolution flow cytometry. This outstanding feature provides a reduced footprint in the μm-scale (versus the mm-scale lateral sizes of previous designs [37]), offering a versatile and ultra-compact approach for building microflow cytometers through the scheme shown in Fig. 1(c) [17]. In order to determine the quality and performance of flow cytometry-based devices, two of the most relevant parameters are the SNR and the CV. The SNR quantifies the variation in the retrieved signal (voltage or power) when a target is illuminated by a light

Optics EXPRESS

beam, in relation to a baseline configuration with no targets (noise). On the other hand, the CV stands for the ratio of the standard deviation to the mean of the light signal intensity retrieved for all the events detected during a time lapse for a single direction [5]. While the SNR is altered by the experimental performance of the microfluidic and optical subsystems as well as by the electronic devices handling the data processing, numerical simulations can provide accurate qualitative and quantitative information regarding this parameter. However, it must be pointed out that attaining the CV via simulations would be useless since the standard deviation of the scattered light signal of a particle in a single direction will always be zero, yielding an ideal (and unreal in experiments) CV = 0% (hence, this parameter was only retrieved from experimental data).

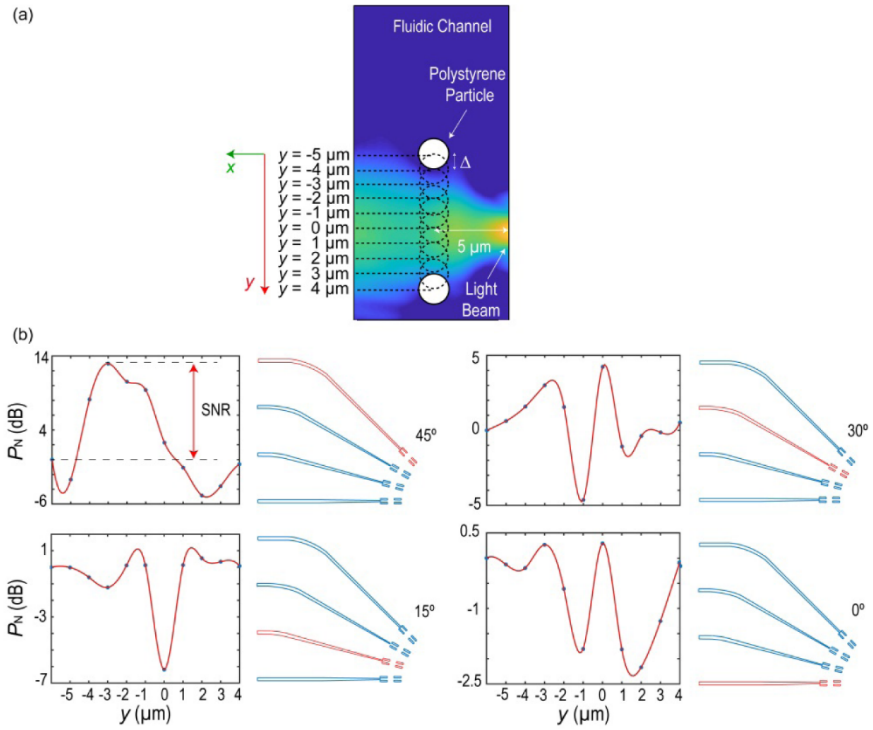

Fig. 2. 3D simulations of the electromagnetic power scattered by polysterene microspheres performed with the CST Microwave Studio Suite commercial software. (a) Schematic top view of a microfluidic channel where a polystyrene bead is flowing. The light beam radiated by the emitting antenna illuminates the targets (at the center of the channel in the transverse or x-direction) for ten different longitudinal positions, from $y = -5$ µm to $y = 4$ µm, with steps of $\Delta = 1$ µm. In an experiment, a flowing particle will be in a different position at each instant. Therefore, the pulse obtained by simulating the power received as a function of these set of positions represents a discretized version of the pulse received at the detector as a function of time as a microsphere passes in front of the antenna (up to a horizontal scale factor that depends on the particle speed). (b) The power P scattered from the target at each of the 10 positions shown in Fig. 2(a) (events) is retrieved for each receiving antenna. The value of $P_N = 10 \cdot \log 10\ (P/P_B)$ associated with each event is represented as a solid circle (P_B accounts for the power of the baseline configuration when no targets are within the channel). The resulting set of circles is interpolated by a red curve, obtaining a different characteristic pulse shape for each of the analyzed reception angles.

It is well-known that a given particle scatters light differently in each direction. Therefore, the power intensity detected by the receiving antenna depends on the angle at which it is placed. One of the goals of this work was to optimize this angle in order to maximize the SNR. To this end, we simulated the power received in a set of antennas placed at different

Optics EXPRESS

angular directions, which were normalized to the power received in the baseline configuration (i.e., that in which there is no particle in the channel between antennas). The complete considered system consists of an emitting antenna, a 10-μm-wide 4-μm-deep fluidic channel filled with an aqueous solution through which particles flow, and the aforementioned set of receiving antennas. To find the optimal system configuration, we explored the scattered-power signature of polystyrene microspheres (with a diameter of 2 μm), the standard test beads in flow cytometry. In particular, we considered a hub of antennas with an angular separation of 15 degrees (taking the center of the microchannel as the origin). While the study of more angular steps could provide a more accurate estimation of the optimum angle, the particularly time-consuming 3D simulations required to this end (besides the large 3D simulation domain containing all the involved optical elements, one has to calculate the fields for a considerable number of microparticle positions for each receiving direction) led us to consider this assumable set of directions, which, as we will show below, is enough to obtain a dramatic enhancement of the SNR. Additionally, from an experimental perspective, the chosen step helps us to avoid fabrication limitations and potential errors. Using the configuration shown in Fig. 1(c), polystyrene beads were placed in the middle of the microfluidic channel (x- and z-direction), while different positions in the flowing direction (y-axis) were considered, starting 5 μm away from the emitting antenna position, see Fig. 2(a). At $y = \pm 5$ μm, the received power approximately corresponds to the noise level (no microparticle), with further distances providing similar results.

The power scattered at the previously mentioned set of antennas placed at 0°, 15°, 30° and 45°, was numerically retrieved for bead positions from $y = -5$ μm to $y = 4$ μm in small increments of $\Delta = 1$ μm, see Fig. 2(b). Regarding the antenna placed at 60°, an extremely low level of intensity below the measurable noise threshold of our laboratory equipment was attained for the baseline configuration, leading us to dismiss this option (and larger angles) in the final set of receiving antennas. Moreover, as obviously expected, antennas placed in a mirrored configuration with respect to the emitting antenna (–15°, –30° and –45°), yielded very similar pulse shapes to those measured for their positive-angle counterparts, not providing additional information of the targets. This feature reduced the angles to be explored to the four previously mentioned directions. As can be seen in Fig. 2(b), there are different and characteristic pulses depending on the direction from which the scattered field of the particle is retrieved. Clearly, the better SNR was attained for the 30° and 45° directions, with a value of ≈5 dB for the former and an outstanding ≈13-dB figure for the latter. The amplitude and well-defined pulse shape associated with this direction promises to provide the most efficient target identification, yielding unequivocal time-dependent signatures. In particular, it approximately provides a 10-dB enhancement with respect to our previous design, in which a 30° angle was considered for the receiving antenna [17]. This numerical enhancement turned out to be slightly better at the experimental level (see below). To better understand how the particles scatter light when passing through the radiated beam, we numerically calculated the two-dimensional power distribution on the xy plane (centered along the z-direction with respect to the antennas) associated with polystyrene beads located at several positions for the 45° configuration; see Figs. 3(a) and 3(b). The enhancement of the signal at the receiving antennas is notable for a certain target location ($y = -3$ μm), justifying the results of Fig. 2.

Optics EXPRESS

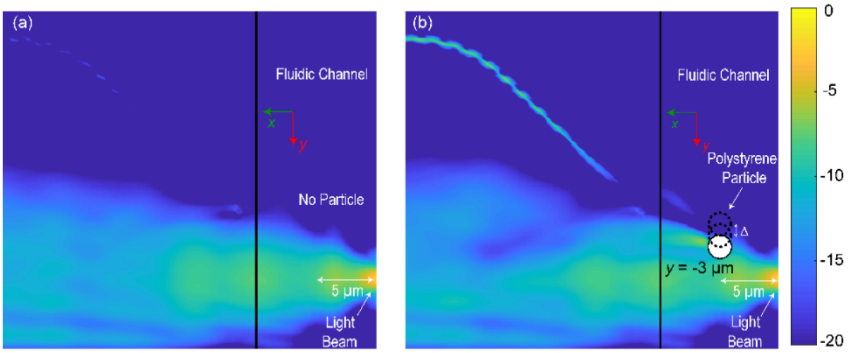

Fig. 3. Two-dimensional distribution of the power intensity when no targets are flowing through the channel (a) and when the target is located at $y = -3$ μm for the 45° receiving antenna configuration (b). Note that the color bar stands for the power intensity (dB) normalized to the maximum power displayed in these 2D cross sections.

While the subsequent experimental results suggest that particles approximately flow along the channel center line, in order to analyze the influence of a possible offset of the particle position in the x and z directions, we performed additional simulations in which the particle center was assumed to move along a line with coordinates $x = x_0$ and $z = z_0$ ($x_0 \neq 0$ or $z_0 \neq 0$), for both the 30° and 45° cases. Figure 4 shows the corresponding simulated pulses. As can be seen, the pulse shape is similar to that of the $x_0 = 0$, $z_0 = 0$ case for some offset values, but varies significantly for other ones. To avoid this variation, the particle must be forced to flow as close as possible to the channel center. This is a basic requirement for flow cytometers, as it also ensures that particles flow in line, preventing multiple particles from going through the light beam simultaneously. It has been demonstrated that this feature can be readily achieved in microflow cytometry via hydrodynamic focusing, based, e.g., on the concept of Dean flow and the use of curved microfluidic channels, which can be fabricated using standard soft lithography [19] and seamlessly incorporated to the studied cytometer.

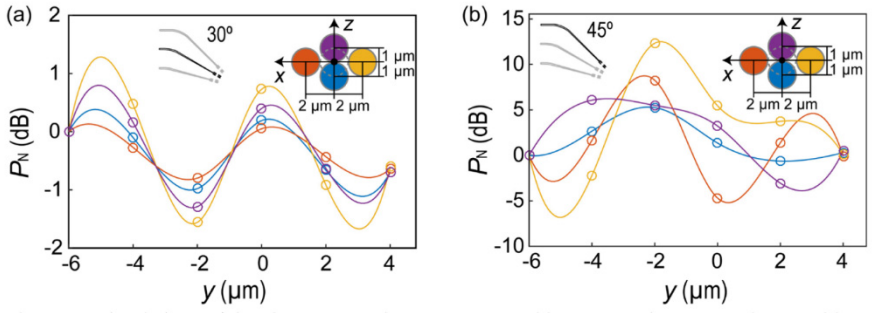

Fig. 4. 3D simulations of the electromagnetic power scattered by 2-μm polysterene spheres, with $x_0 \neq 0$ or $z_0 \neq 0$. Four different cases were considered: $x_0 = 2$ μm, $z_0 = 0$ μm (orange); $x_0 = -2$ μm, $z_0 = 0$ μm (yellow); $x_0 = 0$ μm, $z_0 = 1$ μm (purple); $x_0 = 0$ μm, $z_0 = -1$ μm (blue). (a) Power received at the 30° antenna. (b) Power received at the 45° antenna.

3. Experimental results

Taking into account the previous discussion, we conducted an experiment to demonstrate the large SNR values of the proposed microflow cytometer. In our final device, the wireless deployment is made up of the highly-directive emitting antenna considered above and two other identical antennas measuring the scattered field at 30° and 45° (the angles for which a better numerical SNR was obtained), see Fig. 5(a). Another antenna placed at 0° was included for calibration purposes. Input and output grating couplers enabled vertical light injection

Optics EXPRESS

(extraction) to (from) the chip [38]. To build the fluidic subsystem, a 10-µm-wide 4-µm-deep trench was directly opened in the SiO_2 region in between the antennas (see the fabrication section below for more details). This subsystem is completed with the incorporation of two inlet and outlet reservoirs; see Fig. 5(b). These structures enable the casting of the solutions within the microfluidic channel, allowing the particles to flow in front of the nanoantennas. Finally, a 150-µm-thick polydimethylsiloxane (PDMS) layer was placed atop this configuration, sealing the device and assuring that the targets do not overflow the fluidic path.

As a consequence, capillary forces ensure that the solution reaches the microchannel and flow the targets between the antennas. To test the device, we used the aforementioned 2-µm polystyrene microspheres in an aqueous solution (10 µl volume, concentration of 0.1% solids). As noted above, the reason for using this kind of particle is that they are usually employed as benchmarks for calibrating commercial flow cytometers. Particles were injected into the microfluidic channel by means of a manual drop casting on the inlet reservoir with a high-precision micropipette. Since the aim of this work was to improve the SNR by exploring the target time-dependent scattering signature at different angles, achieving high flow rates was unnecessary (note that the employed scheme does not impose an upper limit for the flow rate, as the scattered power pattern is not affected by the particle speed). Therefore, we designed a basic microfluidic system not including an automated syringe-based pumping flow control. Nevertheless, an external pumping system could be easily included in our device. With this addition, and using a standard high-speed acquisition system (sampling rate in the MHz range) [19], throughput values of the order of thousands of particles per second can be potentially achieved under the conditions of this study [5,19]. On the other hand, a high particle concentration could affect the scattered radiation pattern if two consecutive particles in close proximity go through the light beam. Thus, this parameter should be kept under a

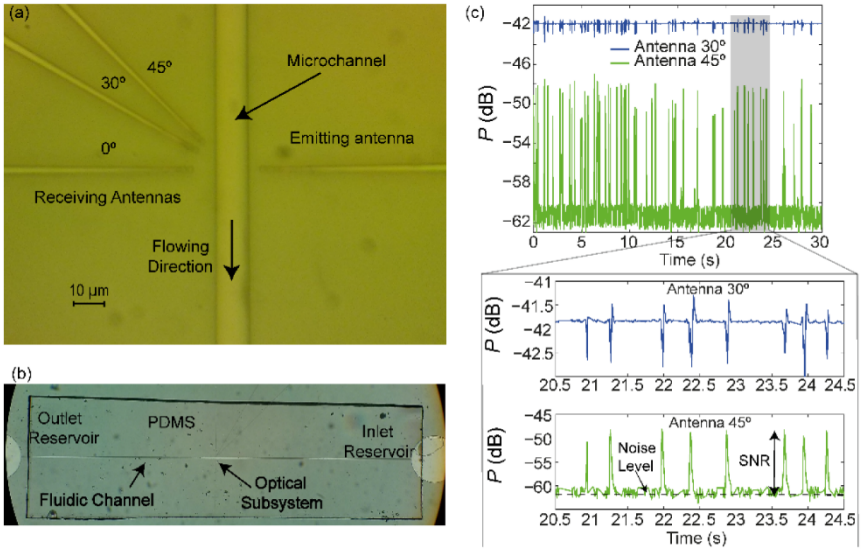

Fig. 5. (a) Optical microscope image of the fabricated microflow cytometer. (b) Optical microscope image of the complete device (except for the grating couplers), including the reservoirs and the microfluidic channel. The border of the top PDMS layer is also displayed. Note that, at this scale, the position of the optical system is not visible. (c) Power efficiency (P) simultaneously measured at 30° and 45° during a four-second interval. In this case, $P = 10 \cdot \log 10\ (P_{RX}/P_{TX})$, where P_{TX} is the power injected to the emitting antenna, and P_{RX} is the power retrieved at the receiving antennas. Very similar pulse shapes are measured if compared with those calculated numerically (Fig. 2). The SNR level for the 45° configuration also matches the results anticipated by the simulations.

Optics EXPRESS

certain threshold. Another possibility would be to train the classification system (see below) to recognize multi-particle events. The two receiving antennas located at 30° and 45° simultaneously retrieved the characteristic time-dependent scattered-field pulses of these beads as passing in front of the emitting antenna. Focusing on the 45° direction, a well-defined pulse is displayed at each detection event, see Fig. 5(c), yielding SNR figures as high as 14 dB (noise level of −62 dB). Outstandingly, there is an almost qualitative and quantitative perfect agreement between the simulations and the experimental results.

Regarding the 30° direction, the time-dependent shape of the measured pulses was very similar to that of the previous numerical analysis. In particular, the pulse slightly grows at the beginning, then displays a pronounced inverted ramp, and finally grows again; see Fig. 5(c). The qualitative agreement between both simulations and experiment is clear, while displaying some amplitude differences. These results show the importance of choosing a suitable angle for the receiving antenna. In particular, we obtain an SNR improvement of more than 10 dB with respect to our previous experiment just by changing this angle from 30° to 45°. In addition, we calculated the experimental CV for both cases, yielding values of 28.17% and 6.64% in the 45° and 30° directions, respectively. This last figure entails a record regarding the reported CV for previous microflow cytometers where the light signal is retrieved on-chip. Outstandingly, the conducted experiments prove that the ultra-directive beams radiated by the employed nanoantennas are crucial to resolve very small particles, offering a simple route towards sub-micron POC biotarget analysis. Moreover, the obtained state-of-the-art figures of SNR and CV demonstrate that this device might be a suitable solution in the field of ultra-integrated low-cost flow cytometers, in contrast to current large-footprint on-chip versions or bulky and expensive commercial devices.

Finally, we additionally retrieved the characteristic pulse shape at different angles for 1-µm polystyrene microparticles, proving that, despite being optimized for 2-µm microspheres, the 45° configuration also renders the best performance in terms of SNR for various types of particles, see Fig. 6. The unique scattering signature of a given kind of particle can be used to achieve a highly-selective (ultimately specific, defined as 100% selective) detection, i.e., to detect such kind of particle in mixtures without interferences from other components of similar behavior. Depending on the case, the mentioned signature can be inferred from the information obtained at a single angle, while more angles could be required in matrices with complex populations. Usually, the scattering is sampled at one or two angles, known as the forward scattering and the side scattering [5, 32]. In both cases, the present study would allow us to select the angles that maximize the SNR. There exist different algorithms to classify the flowing particles from the retrieved scattering information, such as supervised machine learning [25]. Here, the signatures of a set of particles (representative of the populations of interest) whose class is known a priori would be used to train and test the classifier. After this process, the device is able to predict the class of each component in a real sample. Other algorithms employed in classification include principal component analysis and linear discriminant analysis [39].

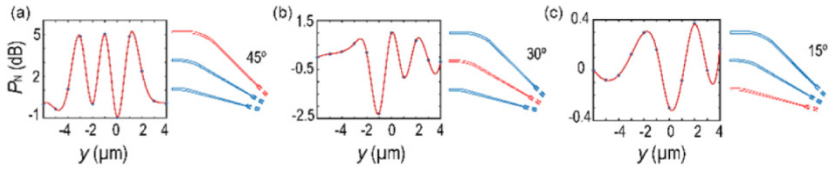

Fig. 6. (a), (b), (c) Different pulse shapes were simulated at different angles for 1-µm polystyrene targets, in analogy to the 2-µm microspheres case shown in Fig. 2(b).

4. Materials and methods

The silicon antennas, waveguides and grating couplers were fabricated on standard SOI samples from SOITEC wafers with a top silicon layer thickness of 220 nm (resistivity ρ ~1-10

Optics EXPRESS

$\Omega \cdot cm^{-1}$, with a lightly p-type background doping of ~10^{15} cm^3) and a buried oxide layer thickness of 2 µm. The fabrication is based on an electron-beam direct-writing process performed on a coated 100 nm hydrogen silsesquioxane (HSQ) resist film. The mentioned electron-beam exposure, performed with a Raith150 tool, was optimized in order to reach the required dimensions employing an acceleration voltage of 30 KeV and an aperture size of 30 µm. After developing the HSQ resist using tetramethylammonium hydroxide, the resist patterns were transferred into the SOI samples employing an optimized Inductively Coupled Plasma-Reactive Ion Etching process with fluoride gases. Finally, a two-micron-thickness silicon dioxide upper cladding was deposited on the SOI sample by using a Plasma Enhanced Chemical Vapour Deposition system from Applied Materials. Regarding the fabrication of the fluidic channel, a Cr layer of 35 nm was first deposited on the SOI sample by using electron beam metal evaporation. Next step consist of a direct writing electron beam exposure of the channel on a layer of 100 nm of PMMA 950K positive resist. After resist developing, Cr was removed from the channel area using a wet Cr etchant process based on CR-7 ($HClO_4$ + $C(NH_4)_2(NO_3)_6$ + H_2O). Subsequently, an ICP-process was carried out to dig the channel through the SiO_2. Finally, the sample was cleaned to remove the organic residues by a mixture of H_2SO_4 and H_2O_2 (3:1) during 20 minutes and then washed by deionized water (DIW). This cleaning procedure was also used to regenerate the device after sensing experiments. To prepare the 150-µm thick PDMS substrates (Sylgard 184 Silicone Elastomer Down Corning), the PDMS mixture (10:1) was spin-coated on glass cover slides and cured at 60°C during 1 hour to obtain the aforementioned PDMS layer on the glass slide. In order to clean the surface, after the healing process, the PDMS was peeled off from a glass slide and washed in absolute ethanol. Finally, the PDMS substrate was positioned and aligned atop the fluidic channel granting its sealing.

It is worth mentioning that, while e-beam lithography (employed here to provide a device proof of concept) is not a cost-effective large-scale production approach, other techniques such as nanoimprint lithography can also achieve the resolution required to fabricate the proposed microflow cytometer and are suitable for mass manufacturing [40].

5. Conclusions

In this work, we have experimentally demonstrated the realization of an on-chip silicon photonic antenna-based microflow cytometer with a notably improved SNR in the target detection, yielding figures as high as 14 dB. Outstandingly, this design is achieved with a dramatically reduced footprint (0.64 × 14 μm^2 for a single antenna), when compared with current state-of-the-art approaches [5]. This feature becomes especially relevant in the future realization of integrated multi-testing systems [41], allowing a cell/biotarget to flow along several analysis stages on the same chip. As a reference, we can compare some of the most relevant parameters of the device here proposed with the typical specifications of standard commercial devices. For instance, the flow cytometers of the Beckman Coulter FC 500 series (used for benchmarking e.g. in [19]) are able to resolve 0.5 µm particles (a value achievable with our device thanks to the aforementioned high directivity of the employed nanoantennas), show a CV between 2% and 4% (the best result for our device is ≈6%), and offer a maximum acquisition rate of 3300 events/second (potentially reachable by the studied cytometer, see our discussion above). In this respect, our device shows a competitive performance in comparison with commercial cytometers. Moreover, the use of the SOI platform in the fabrication of the antennas readily ensures the mass production of these devices.

Nevertheless, besides improving the microfluidic system to incorporate the aforementioned advanced features, reaching the commercial stage would still entail a series of steps, including chip packaging as well as the development of the required control/processing electronics and of the appropriate application-specific classification algorithms.

The combination of the proposed antenna-based photonic subsystem together with integrated microfluidic set-ups paves the way to the realization of ultra-compact low-cost lab-

Optics EXPRESS

on-a-chip flow cytometers and POC sensing devices with a direct impact for biological, chemical and medical diagnosis. Additionally, nanoparticle-counting systems [42, 43], which are also related to allergen detection or industrial food processing tests, might be tremendously improved thanks to these cost-effective ultra-integrated devices.

Funding

Funding from grant TEC2015-63838-C3-1-R OPTONANOSENS (MINECO/ FEDER, UE) is acknowledged. C.G.-M. acknowledges support from project TEC2015-73581-JIN PHUTURE (AEI/FEDER, UE). This work was also supported by the EU-funded projects FP7-ICT PHOXTROT (No.318240), the EU-funded H2020-FET-HPC EXANEST (No.671553) and the Generalitat Valenciana's PROMETEO grant NANOMET PLUS (PROMETEO II/2014/34).

Acknowledgments

We thank David Zurita for his help in the design of the data acquisition code for the sensing application.